

Feeding a Molecular Squid: A Pliable Nanocarbon Receptor for Electron-Poor Aromatics

Rafał Frydrych, Tadeusz Lis, Wojciech Bury, Joanna Cybińska, and Marcin Stępień*



Cite This: *J. Am. Chem. Soc.* 2020, 142, 15604–15613



Read Online

ACCESS |



Metrics & More

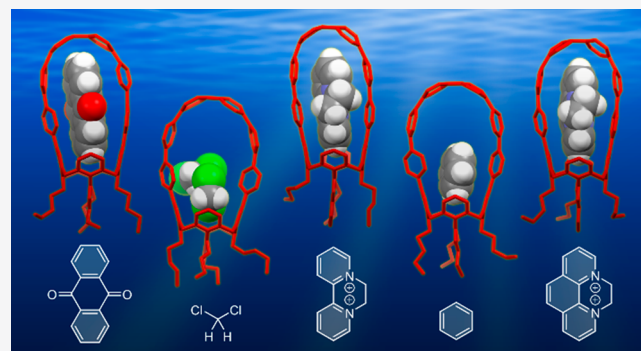


Article Recommendations



Supporting Information

ABSTRACT: A hybrid nanocarbon receptor consisting of a calix[4]arene and a bent oligophenylene loop (“molecular squid”), was obtained in an efficient, scalable synthesis. The system contains an electron-rich cavity with an adaptable shape, which can serve as a host for electron deficient guests, such as diquat, 10-methylacridinium, and anthraquinone. The new receptor forms inclusion complexes in the solid state and in solution, showing a dependence of the observed binding strength on the shape of the guest species and its charge. The interaction with the methylacridinium cation in solution was interpreted in terms of a 2:1 binding model, with $K_{11} = 5.92(7) \times 10^3 \text{ M}^{-1}$. The solid receptor is porous to gases and vapors, yielding an uptake of ca. 4 mmol/g for methanol at 293 K. In solution, the receptor shows cyan fluorescence ($\lambda_{\text{max}}^{\text{em}} = 485 \text{ nm}$, $\Phi_{\text{F}} = 33\%$), which is partly quenched upon binding of guests. Methylacridinium and anthraquinone adducts show red-shifted emission in the solid state, attributable to the charge-transfer character of these inclusion complexes.

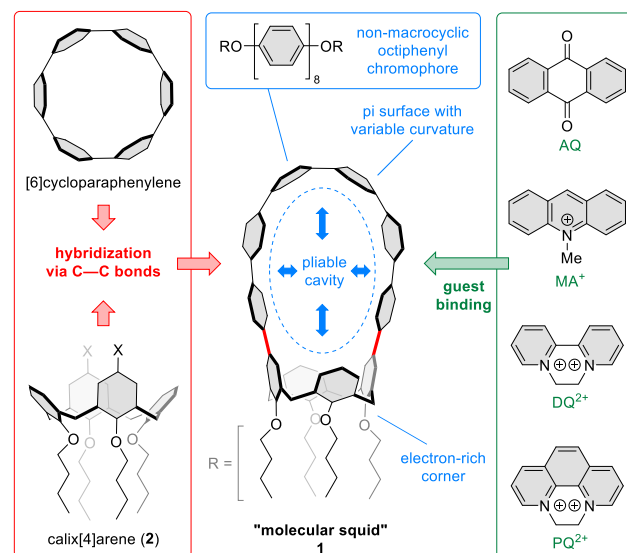


INTRODUCTION

Curved aromatic molecules have found diverse uses in supramolecular and nanomaterials chemistry.^{1–3} In particular, carbon-rich cavities of such systems have been used to develop cylindrical,^{3–11} concave,^{12,13} and macrocyclic hosts^{14,15} for spherical guest molecules and ions, self-assembling surfaces,^{16,12,17} and porous organic materials.^{18,19} In these systems, the receptor function can be precisely controlled by the type and extent of curvature and by adjusting the cavity dimensions. The curvature facilitates formation of interlocked structures, i.e., rotaxanes,^{20,21} catenanes,^{22–25} and molecular knots.²⁴ While the synthesis of curved aromatics is often challenging,²⁶ they provide structural rigidity, variable curvature types,^{27–29} topologically nontrivial π conjugation,^{23,30–32,19} chirality,³³ and unusual chromophore properties.^{34–36} These features can be leveraged to enhance supramolecular interactions and to produce usable physical output upon self-assembly.³⁷

Cycloparaphenylenes (CPPs) have played a major role in these advances since the development of efficient synthetic methods based on masked phenylene equivalents^{38,39} and metallacycle eliminations.⁴⁰ In particular, new supramolecular functions have been produced by hybridization of oligophenylene nano-hoops with other building blocks such as porphyrins,¹⁰ perylene diimides,^{41,42} electron-rich arene substructures,^{43–45} perfluorinated rings,^{46,47} and N-donor heterocycles.^{21,23} Here we report on a calixarene–CPP hybrid (**1**, Chart 1), in which the calixarene and oligophenylene units are directly linked via CC bonds. This squid-shaped molecule has

Chart 1. Design of the Molecular Squid^a



^a π -Conjugation in **1** and its parent motifs is omitted for clarity.

Received: July 29, 2020

Published: August 20, 2020

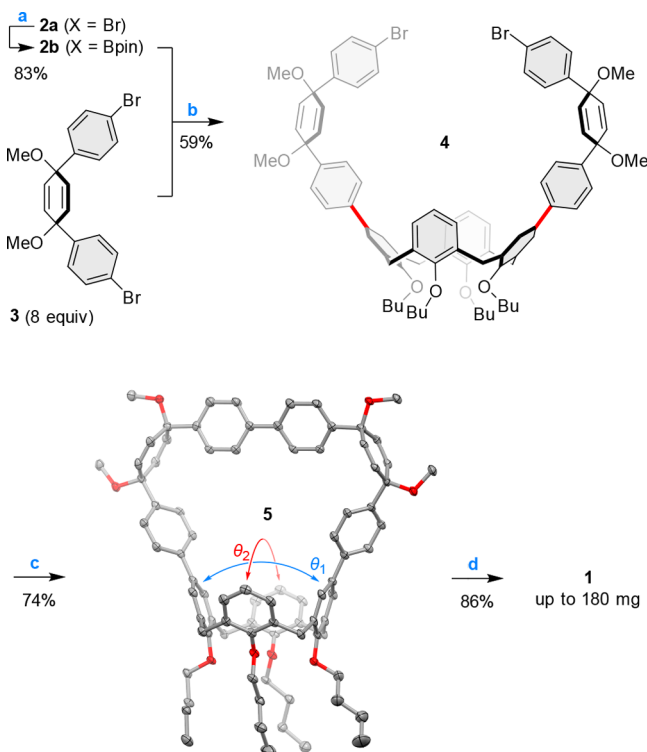


a flexible cavity and can bind neutral and cationic guests both in solution and in the solid state.

RESULTS AND DISCUSSION

Synthesis. Compound **1** was prepared from the diagonally functionalized dibromocalix[4]arene **2a**, which can be obtained stereoselectively as a cone-like structure (Scheme 1).⁴⁸ **2a** was

Scheme 1. Synthesis of **1**^a



^aReagents and conditions: (a) Pd(dppf)Cl₂ (0.05 equiv), [B(pin)]₂ (2.4 equiv), CH₃COOK (2.4 equiv), dioxane, 110 °C, 12 h; (b) Pd(OAc)₂ (0.12 equiv), dppf (0.135 equiv), Ag₂O (4.5 equiv), K₂CO₃ (2 equiv), toluene, water, 80 °C, 24 h; (c) Ni(cod)₂ (2.5 equiv), 2,2'-bipyridyl (2.5 equiv), THF, DMF, 80 °C, 16 h; (d) H₂SnCl₄ (8 equiv), THF, rt, overnight.

borylated and coupled with Jasti's masked phenylene building block **3**,³⁸ and the resulting dibromo intermediate **4** was cyclized using Yamamoto coupling, to furnish the basket-like precursor **5**. The molecular structure of **5**, revealed by an X-ray crystallographic analysis, is characterized by slight bending of the lateral biphenyl sections of the loop, indicative of a small degree of internal strain. The interplanar angles between the diagonal pairs of benzene rings in the calixarene section of **5** are respectively $\theta_1 = 33.8^\circ$ and $\theta_2 = 76.9^\circ$ (Scheme 1). These are angles different in the parent calix[4]arene⁴⁹ (**2** with X = H, $\theta_1 = -24.2^\circ$ and $\theta_2 = 68.6^\circ$), indicating that the observed conformation of **5** is a compromise between the steric requirements of the constituent subunits. Reductive aromatization of the two masked *p*-phenylene units in **5** was performed using a tin(II) reagent, as reported by Yamago et al.⁵⁰ Under these conditions, **5** cleanly produced the target **1**, which was isolated in an 86% yield as a yellow solid. Using the above approach we were able to prepare up to 180 mg of **1** in a single batch. The product was unambiguously identified using NMR spectroscopy and mass spectrometry (Figures S48, S49, and

S54; Scheme S4 of the Supporting Information, SI), and was further characterized crystallographically in the solid state (see below).

Molecular Structure. **1** is a flexible molecule, balancing the conformational preferences of the calixarene part with the distortion of the oligophenylene loop. An automated conformational search^{51–53} performed for the simplified structure **1'** (R = ethyl), followed by a full DFT reoptimization of the resulting ensemble, revealed a structural bistability of the oligophenylene loop, which adopted either an elongated (flattened) or circular (rounded) shape (Figure 1). The

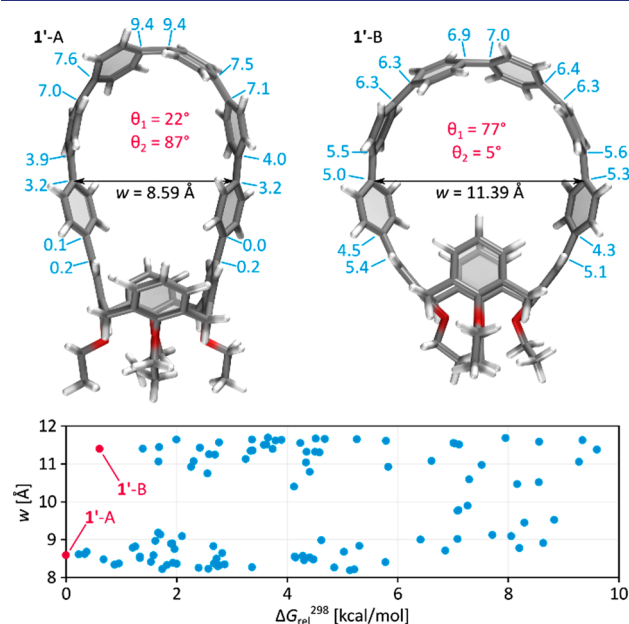


Figure 1. Top: Lowest-energy elongated (A) and rounded (B) conformations of **1'** (R = Et) found in a gas-phase DFT calculation. The initial ensemble of 113 conformers was generated using CREST⁵¹ with an energy cutoff of 6 kcal/mol, and reoptimized at the B3LYP-GD3BJ/6-31G(d,p) level of theory. Bottom: dependence of loop width *w* as a function of Gibbs free energy. θ_1 and θ_2 angles are defined in Scheme 1. POAV angles (blue, degrees) are given for quaternary phenylene carbons. θ_1 and θ_2 angles are defined in Scheme 1.

change of the loop shape is made possible by the flexibility of the calixarene unit, which can switch between two non-equivalent flattened cone conformations. The calculations predict the flattened geometry (**1'-A**) to be preferred in the gas phase, but rounded conformers are nevertheless thermally accessible with the lowest-energy structure (**1'-B**) with a $\Delta G_{\text{rel}}^{298}$ of only 0.6 kcal/mol. Structures similar to **1'-B** are characterized by a more uniform curvature of the oligophenylene substructure with POAV1 angles⁵⁴ in the range of 4.3° to 7.0° . The broader distribution of POAV1 angles found in the **1'-A** conformation is similar to those found in the [16]CPP lemniscate (CPPL) and related systems.^{30,19} The internal strain enthalpy of **1'-A** was estimated as 43.9 kcal/mol in a homodesmotic calculation (Scheme S3). This value is less than half the enthalpy reported for CPPL (102.7 kcal/mol),³⁰ suggesting that the octiphenyl substructure of **1'** is somewhat less strained than each of the two lobes of CPPL.

The pliable internal cavity of our molecular squid is of interest as a potential binding site for guest molecules and ions. An initial indication of the receptor capabilities of **1** was

observed in its two crystalline solvates, $1 \cdot 3.2\text{CH}_2\text{Cl}_2$ and $1 \cdot 3\text{C}_6\text{H}_6$ (Figure 2A,B). The former of these two structures

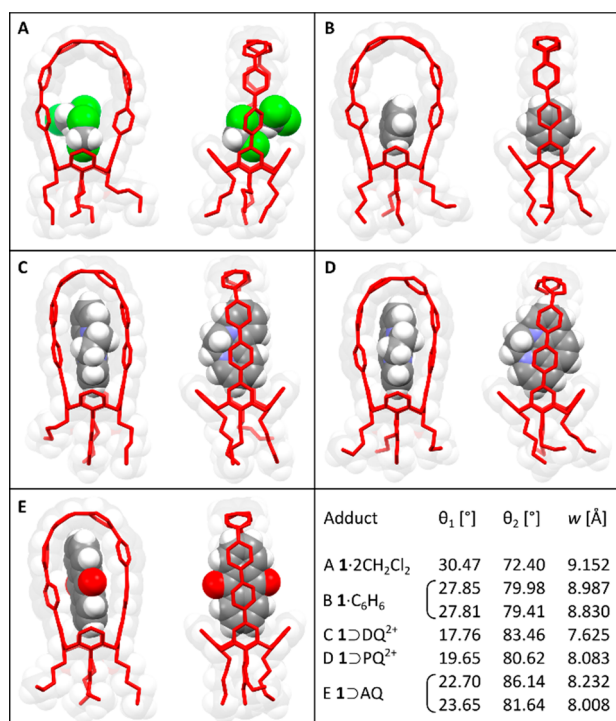


Figure 2. Inclusion complexes of **1** with neutral and cationic guests, observed in the solid state. One of two symmetry-independent complexes is shown for $1 \cdot 3\text{C}_6\text{H}_6$ and $1 \supset \text{AQ}$. Hydrogen atoms (on **1**), solvent molecules (outside cavities), counteranions (for cationic guests), and minor disordered positions are omitted for clarity.

contains a benzene molecule bound in the calixarene end of the cavity. The remaining solvent molecules are located outside the loop, while the loop itself is penetrated by butyl chains of a neighboring molecule. Although not isomorphous, the dichloromethane solvate shows similar features, with an aggregate of two solvent molecules residing in the calixarene cavity, and extraneous alkyl substituents inside the oligophenylene unit. The solvation pattern observed in these two crystals resembles the reported solvates of nanotube end-caps.^{55,56} In each solvate, **1** adopts a flattened conformation ($w = 9.0$ to 9.2 Å), similar to the I' -A structure predicted in the gas phase. This particular conformer contains a larger free volume inside the calixarene corner of the loop, offering more space for inclusion of solvent molecules.

Host–Guest Chemistry in the Solid State. An initial computational search showed that electron-deficient polycyclic aromatics containing three or four fused rings may be suitable as guests for the cavity of **1**. In particular, the interior of the molecular squid was expected to share some of the binding characteristics of the parent CPP and calixarene motifs, displaying an affinity for electron-deficient and positively charged π -conjugated guests. The four guests used for further study (Chart 1), namely anthraquinone (AQ),^{57–59} 10-methylacridinium (MA^+),^{60–65} diquat (DQ^{2+}),^{66–90} and its phenanthroline-derived benzologue PQ^{2+} ,^{89–92} were selected on the basis of their established utility in supramolecular chemistry. As we found, crystals of an inclusion complex could be successfully grown from a dichloromethane solution of **1** and 4 equiv of anthraquinone (AQ) by slow diffusion of

methanol vapors. X-ray crystallographic analysis (Figure 2E) revealed the formation of a 1:1 adduct, $1 \supset \text{AQ}$, in which the receptor cavity is filled completely with the anthraquinone molecule. As a consequence of guest inclusion, the octiphenyl loop of **1** becomes somewhat flatter than observed in the solvates ($w = 8.0$ to 8.2 Å), presumably to better accommodate the length of the AQ guest.

Analogous attempts to obtain solid-state adducts by cocrystallization of **1** with organic salts were unsuccessful. In an alternative approach, crystals of $1 \cdot 3\text{C}_6\text{H}_6$ were soaked⁹³ in an acetone–methanol solution of 6,7-dihydrodipyrido[1,2-*a*:2',1'-*c*]pyrazine-5,8-dium hexafluorophosphate (diquat, $[\text{DQ}^{2+}][\text{PF}_6^-]_2$). The dark brown crystals obtained using this method were found to contain the desired complex, $[\text{1} \supset \text{DQ}^{2+}][\text{PF}_6^-]_2$ (Figure 2C). The extreme flattening of the oligophenylene loop observed in the $[\text{1} \supset \text{DQ}^{2+}]$ adduct ($w = 7.6$ Å) is likely caused by a combination of steric, electrostatic, and crystal packing contributions. An analogous crystal-to-crystal transformation could be effected when **1** was similarly treated with 5,6-dihydropyrazino[1,2,3,4-*lmn*][1,10]-phenanthroline-4,7-dium hexafluorophosphate ($[\text{PQ}^{2+}][\text{PF}_6^-]_2$). Interestingly, even though the PQ^{2+} cation is flatter than DQ^{2+} , the loop width w in the $[\text{1} \supset \text{PQ}^{2+}]$ adduct (8.0 to 8.2 Å) is somewhat larger than in $[\text{1} \supset \text{DQ}^{2+}]$.

The crystals formed by solvates and adducts of **1** are not isomorphous, but they nevertheless reveal striking analogies of their packing patterns (Figure 3). Structures of the benzene and dichloromethane solvates consist of herringbone layers characterized by partial penetration of butyl chains into neighboring oligophenylene loops. Packing of these layers is affected by the bulk of calixarene moieties and has no direct relationship with the herringbone patterns observed in unmodified cycloparaphenylenes.⁹⁴ In each solvate, the herringbone direction is antiparallel in consecutive layers. The inclusion of molecules and ions in the adducts of **1** leads to significant expansion of the crystal lattices. Importantly, however, the antiparallel arrangement of layers is preserved in all cases. Individual molecules are collinearly aligned within each layer and the butyl chains no longer penetrate the cavities, which are now filled with the guest species (DQ^{2+} , PQ^{2+} and AQ). In the salt adducts, the PF_6^- anions are sandwiched in between the layers and retain close contacts with the edges of the organic cations. The structural analogies between the solid-state structures of solvates and those of the adducts indicate that the incorporation of DQ^{2+} and PQ^{2+} salts in the lattice is indeed feasible via a direct crystal-to-crystal transformation, as it can occur without major reorientation of the molecules.

Guest Binding in Solution. When solutions of **1** in acetone- d_6 were titrated with hexafluorophosphate salts of DQ^{2+} , PQ^{2+} , and MA^+ , significant changes of chemical shifts were induced in the ^1H NMR spectra, consistent with the formation of host–guest complexes in fast exchange with the free host (Figures 4, S5, S9, S13, and S17). These changes were most pronounced in the aromatic region of the spectrum, but systematic downfield relocations were also observed for all aliphatic signals of **1**. The broadening of guest signals, observed in all three titrations, suggested that the chemical shifts of the bound and free guest differ considerably. This assumption was verified for a sample of **1** containing 1.5 equiv of DQ^{2+} , for which the slow-exchange limit was observed at 174 K in acetone- d_6 (Figure S19). Under these conditions, no free **1** was present in solution, whereas the signals of the bound DQ^{2+} could be readily identified on the basis of the exchange

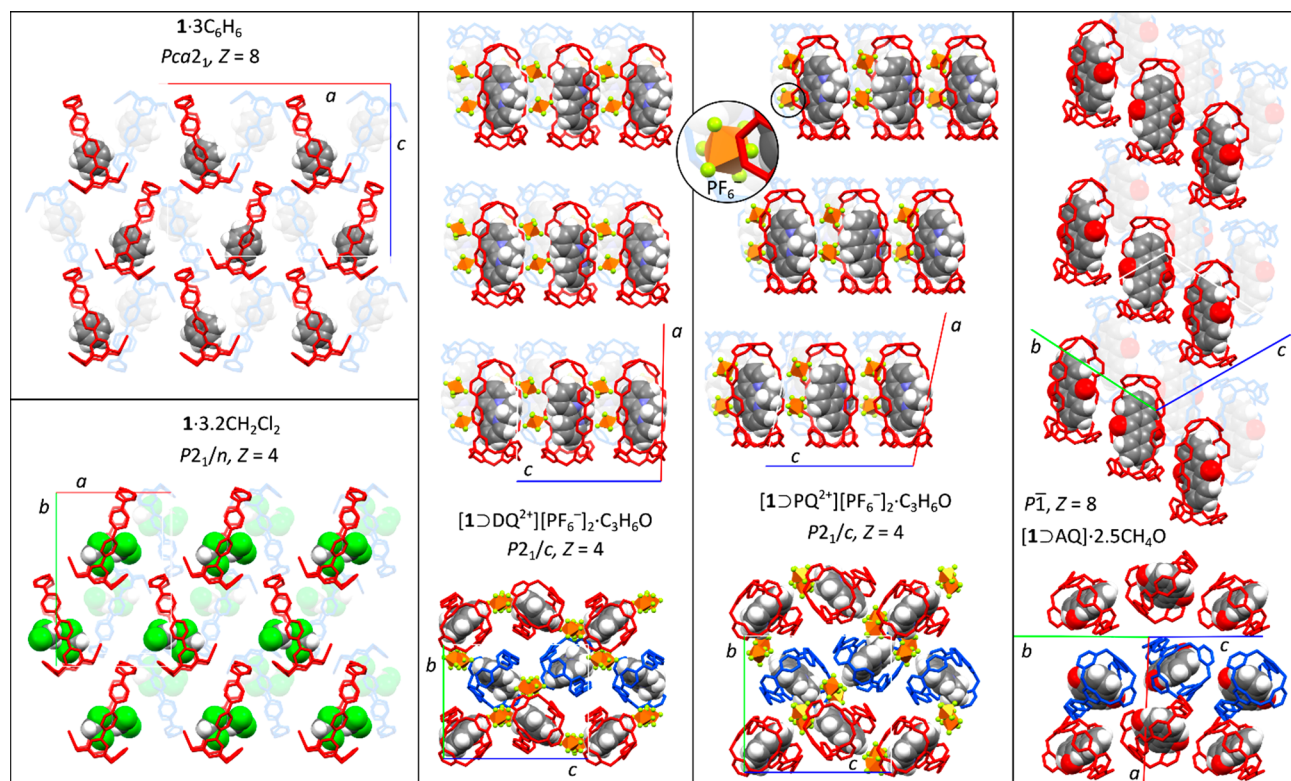


Figure 3. Packing diagrams of inclusion complexes of **1**. Molecules of **1** in adjacent layers are colored in red and blue. Hydrogen atoms and butyl substituents (on **1**), solvent molecules (outside cavities), and minor disordered positions are omitted for clarity.

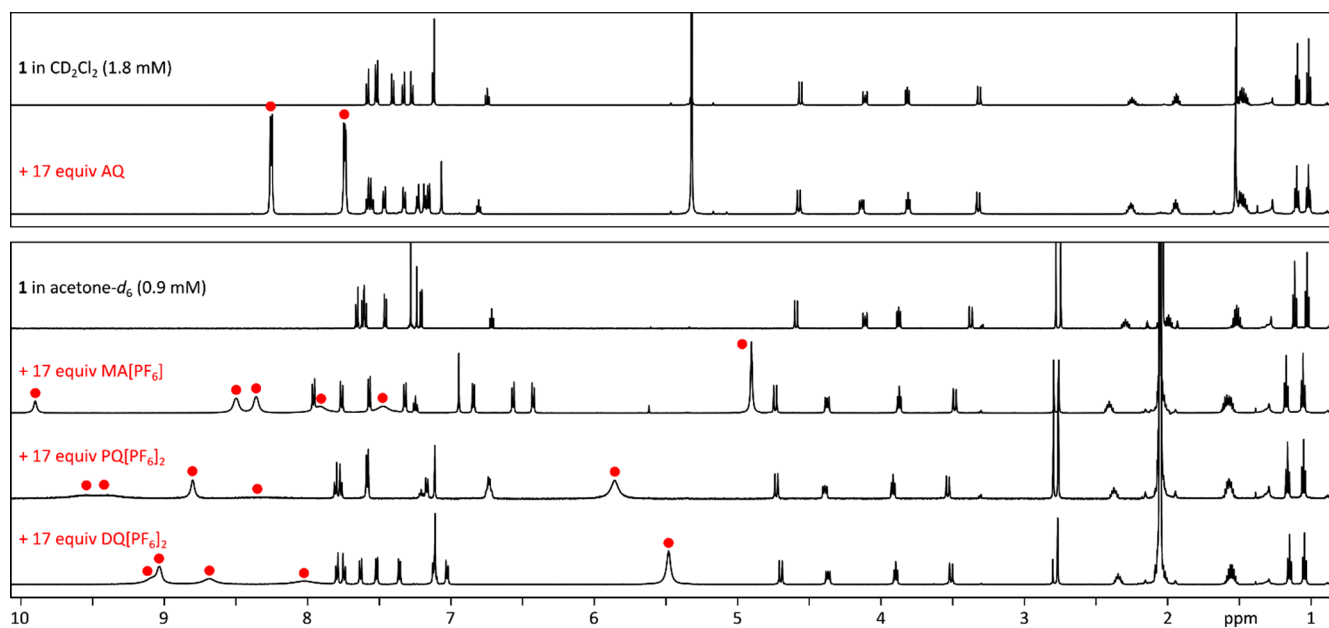


Figure 4. Formation of inclusion complexes of **1** in solution observed using ^1H NMR spectroscopy (600 MHz, 300 K, acetone- d_6 or CD_2Cl_2). For complete titrations, see Figures S5, S9, S13, and S17. Signals of guests are indicated with red bullets.

correlations with the free DQ^{2+} observed in a ROESY spectrum (Figure S22). The shifts of the bound DQ^{2+} were consistently upfield relative to the free DQ^{2+} , reflecting the shielding induced by the aromatic surface of the oligophenylene loop. Interestingly, the spectral pattern of the bound DQ^{2+} is completely desymmetrized, with four signals corresponding to the CH_2CH_2 unit. This low spectral symmetry indicated that not only the “somersault” rotations of DQ^{2+} inside the

host cavity, but also the pseudoinversion of the twisted biaryl backbone were slow on the NMR time scale at 174 K.

While the crystal structures and low temperature NMR experiments provided unambiguous evidence for the formation of binary complexes with cationic guests, binding isotherms obtained from the ^1H NMR titrations produced small but systematic discrepancies when fitted using the simple 1:1 binding model. The fit could be considerably improved by

assuming initial formation of a relatively unstable ternary complex $[1_2\supset X^{n+}]$ (where X^{n+} is the cationic guest),⁸¹ which would be converted into the $[1\supset X^{n+}]$ at higher guest concentrations (Tables 1 and Table S1). Data obtained

Table 1. Association Constants for Host–Guest Complexes of 1^a

guest	model	K_{11} [M^{-1}]	K_{21} [M^{-1}]
DQ ²⁺ ^b	2:1	$6.03(2) \times 10^2$	$3.36(3) \times 10^1$
PQ ²⁺ ^b	2:1	$1.43(1) \times 10^3$	$1.78(4) \times 10^2$
MA ⁺ ^b	2:1	$5.92(7) \times 10^3$	$4.3(1) \times 10^2$
AQ ^c	1:1	$1.968(2) \times 10^1$	

^aBased on ¹H NMR titration data (300 K). ^bIn acetone-*d*₆. ^cIn CD₂Cl₂.

using such a two-step binding model showed that the formation of the ultimate 1:1 species is most efficient for MA⁺ ($K_{11} = 5.92(7) \times 10^3 M^{-1}$), and becomes weaker for PQ²⁺ and DQ²⁺ ($K_{11} = 1.43(1) \cdot 10^3$ and $6.03(2) \times 10^2 M^{-1}$, respectively). In all cases, the K_{21} binding constant is lower by 1 order of magnitude than the respective K_{11} . The strong binding of MA⁺ is likely supported by a favorable combination of the cationic charge with the good geometric match of the guest with the cavity of 1 (Figure 5A). The initial formation of

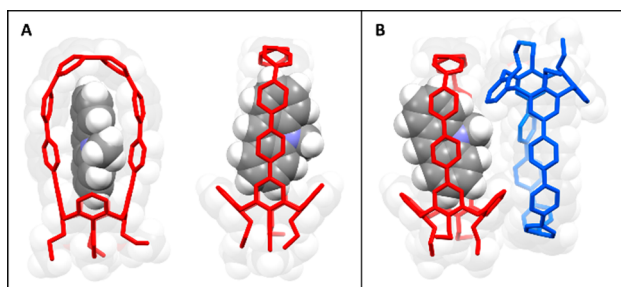


Figure 5. (A) DFT-optimized lowest-energy conformer of $[1'\supset MA^+]$ and (PCM(acetone)/BGD3BJ/B3LYP/6-31G(d,p), initial conformer ensemble obtained using CREST). (B) Lowest-energy conformer of $[1'\supset MA^+]$ found in a CREST metadynamics search.

the ternary complex $[1_2\supset MA^+]$, inferred from the binding isotherm, was probed computationally using a CREST conformational search. Interestingly, the resulting ensemble revealed preferential binding of the cation in a single receptor cavity (rather than across two cavities). Furthermore, in the lowest-energy conformers, the other molecule of 1 was associated with the inclusion complex in an edge-to-edge fashion (cf. Figure 5B). While encapsulation of hexafluorophosphate in the other receptor cavity⁹⁵ could in principle occur to produce the hypothetical species $[1\supset MA^+][1\supset PF_6^-]$, such a binding event was ruled out on the basis of a ¹⁹F NMR titration ($1 + [MA^+][PF_6^-]$, acetone-*d*₆), which showed a negligible effect of 1 on the ¹⁹F chemical shift of the PF₆[−] anion.

A similar though weaker binding interaction was observed between 1 and anthraquinone (AQ) in CD₂Cl₂. In this case, the ¹H NMR titration was fully consistent with the HG (1:1) model ($K \approx 20 M^{-1}$). The formation of the 1:1 adduct was proven using low-temperature ¹H NMR spectroscopy (600 MHz, 160–270 K, CDCl₂F, 4:1 molar ratio of AQ to 1). The use of the latter solvent⁹⁶ instead of CD₂Cl₂ was necessary for direct observation of the host–guest complex in the limit of

slow exchange (Figures S20 and S21). Under these conditions, no free 1 was present, whereas the AQ molecule bound in the $[1\supset AQ]$ complex showed four proton resonances, consistent with an effectively C_{2v}-symmetrical environment of the cavity. Additionally, the EXSY pattern observed between the resonances of free and bound AQ showed that chemical exchange was significant even at 170 K (Figure S23). However, no EXSY peaks were observed among the four resonances of the bound AQ, indicating that the guest is effectively locked inside the cavity of 1, and is not capable of “somersault” rotations at the time scale of the ROESY experiment.

Vapor and Gas Sorption. Gas adsorption analyses performed for a crystalline sample of 1 showed variable porosity toward a range of different adsorbates (Figure 6).

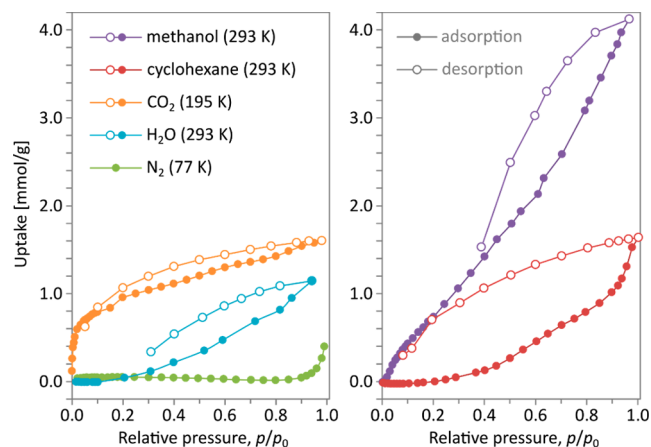


Figure 6. Experimental adsorption and desorption isotherms (solid and empty circles, respectively) of N₂ (77 K), CO₂ (195 K), cyclohexane (293 K), MeOH (293 K), and H₂O (293 K) measured on crystalline sample of 1.

While the N₂ adsorption capacity was very low, significant uptake of CO₂ was observed at 195 K, reaching a maximum of 1.60 mmol/g. This value corresponds to a molar ratio of CO₂ to 1 of ca. 1.8. The BET area, calculated on the basis of the adsorption branch of the CO₂ isotherm, is 63.7 m²/g (Figure S25, Table S2), lower than reported for the larger [12]CPP nanohoop.¹⁸ The isosteric heat of CO₂ adsorption (Q_{st}) was determined for 1 from isotherms measured in the temperature range of 273–293 K, using the single-site Langmuir–Freundlich model and the Clausius–Clapeyron eq (Figures S26 and S27, Table S3). The calculated Q_{st} values reach 53.1 kJ/mol at zero coverage and then decrease to ca. 30 kJ/mol at higher CO₂ uptake. The initial Q_{st} is higher than previously reported for CO₂-selective pillar[5]arene-based sorbents⁹⁷ (up to 44 kJ/mol), implying an energetically favorable interaction between 1 and the initially adsorbed CO₂. The binding enthalpy ΔH^{298} calculated for the inclusion complex $[1\supset CO_2]$ in the gas phase is -48.9 kJ/mol, indicating that the high initial heat of adsorption may indeed correspond to a well-defined supramolecular interaction between CO₂ and 1.

At 293 K, vapor adsorption of H₂O, cyclohexane, and methanol, yielded maximum uptake values of 1.14, 1.64, and 4.12 mmol/g, respectively, corresponding to approximately 1.3, 1.8, and 4.5 adsorbate molecules per one molecule of 1. The significant adsorption hysteresis observed for cyclohexane is indicative of its stronger retention in the pores of 1. On the basis of the MeOH isotherm, a pore volume of 0.167 cm³/g

was estimated for **1**. In comparison, when solvent molecules are removed from the crystal structure model of $1 \cdot 3C_6H_6$, the resulting virtual pores correspond to a helium volume^{98,99} of $0.322 \text{ cm}^3/\text{g}$. The comparatively lower pore volumes attainable via adsorption may indicate that either (a) only part of the virtual porosity of the crystals is available for uptake or (b) a structural reorganization of the material accompanies the sorption process.

Optical Properties. The electronic spectrum of **1** in dichloromethane (Figure 7) features two absorption bands

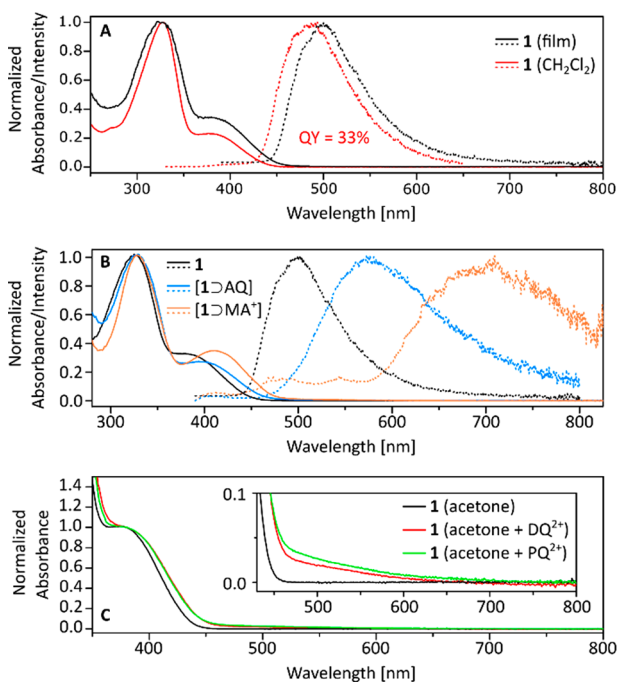


Figure 7. Absorption and emission spectra (solid and dashed lines, respectively) of (A) **1** in dichloromethane solution (red) and as a thin film (black); (B) **1** (black), $[1\supset\text{AQ}]$ (blue), and $[1\supset\text{MA}^+][\text{PF}_6^-]$ (orange) in thin films; (C) **1** in acetone solutions containing (a) no additive (black trace), (b) 178 equiv of $[\text{DQ}^{2+}][\text{PF}_6^-]_2$ (red trace), and (c) 11 equiv of $[\text{PQ}^{2+}][\text{PF}_6^-]_2$ (green trace). The latter two spectra were recorded relative to an acetone solution containing the same amount of the corresponding pure guest.

with $\lambda_{\text{max}}^{\text{abs}} = 327$ and 377 nm , respectively, the latter being responsible for the yellow color of the compound. **1** displays a cyan emission with a maximum at 485 nm and a quantum yield of 33% (in dichloromethane, $\tau_{\text{F}} = 1.82 \text{ ns}$). Similar absorption and emission spectra were observed for amorphous thin films of **1** obtained by drop casting of dichloromethane solutions. Partial quenching of fluorescence was observed during titrations of **1** with molecular and ionic guests, suggesting that charge transfer (CT) may occur between the electron-rich host cavity and the electron-deficient guest molecule. The absorption spectrum of $[1\supset\text{AQ}]$, measured for a thin film, showed a red shift of the lower energy band ($\lambda_{\text{max}}^{\text{abs}} = 396 \text{ nm}$ vs 380 nm for free **1**), and a weak tailing band above 500 nm , not observed in the free **1**, which was tentatively ascribed to a CT transition. Remarkably, the film showed weak yellow-gold fluorescence ($\lambda_{\text{max}}^{\text{em}} \approx 580 \text{ nm}$), red-shifted relative to the solid-state emission of the free host ($\lambda_{\text{max}}^{\text{em}} \approx 500 \text{ nm}$). Similar features were observed in a thin film of $[1\supset\text{MA}^+][\text{PF}_6^-]$, in which an even larger red shift was recorded for the low-energy absorption band ($\lambda_{\text{max}}^{\text{abs}} = 411 \text{ nm}$). Again, a weak absorption

tail was observed, which was complemented by an even more red-shifted emission band ($\lambda_{\text{max}}^{\text{em}} \approx 700 \text{ nm}$), corresponding to the red-orange fluorescence of the film. Good quality films could not be obtained by drop-casting for complexes with DQ^{2+} and PQ^{2+} ; however, when **1** was dissolved in acetone containing a large excess of the corresponding guest, a weak tailing band could be identified in the 450 to 700 nm range, possibly corresponding to CT transitions of the host–guest adducts. For these solutions, there were however no visual indications of any red-shifted fluorescence.

The involvement of charge transfer in the optical spectra of $[1\supset\text{DQ}^{2+}]$ and $[1\supset\text{MA}^+]$ was probed using time-dependent (TD) DFT. The initial geometries were again derived from a CREST metadynamics search and were reoptimized using the PCM(acetone)/CAM-B3LYP-GD3BJ/6-31G(d,p) level of theory, which was also used for the TD calculation. The Coulomb-attenuating method¹⁰⁰ (CAM) was chosen specifically to minimize the self-interaction error, which is known to produce spurious results for CT systems.¹⁰¹ The HOMO and LUMO of **1** are mostly localized on the oligophenylene loop, with vanishing amplitudes on the calixarene subunit (Figure 8).

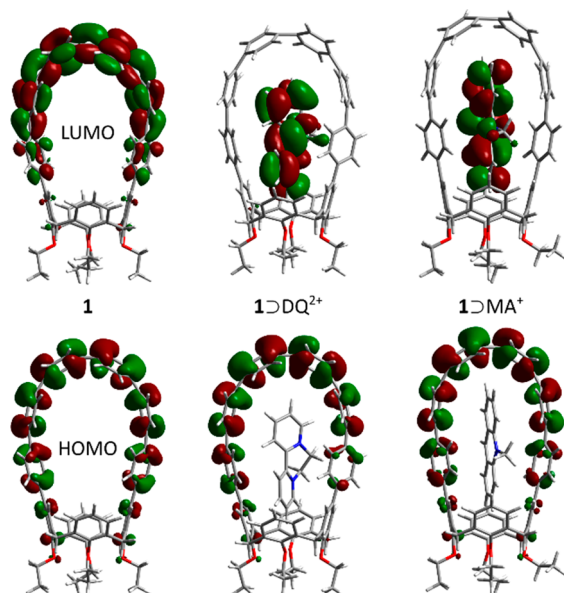


Figure 8. Frontier Kohn–Sham molecular orbitals for **1** and its complexes, $[1\supset\text{DQ}^{2+}]$ and $[1\supset\text{MA}^+]$ (PCM(acetone)/CAM-B3LYP-GD3BJ/6-31G(d,p)).

The adducts of **1** with AQ , MA^+ , DQ^{2+} , and PQ^{2+} retain the HOMO localization of the free host, whereas the LUMO level is always localized on the electron-deficient guest (Figure 8). In $[1\supset\text{DQ}^{2+}]$, the 10 highest occupied Kohn–Sham (KS) MOs are nearly pure orbitals of the host **1**. The three lowest unoccupied MOs (LUMO through L+2) are derived from DQ^{2+} , whereas the L+3 level corresponds to the original LUMO of the host. The calculated absorption profile obtained for the complex is very similar to the experimental one, except for the blue shift of ca. 0.6 eV , characteristic of the CAM method (Figure S34, Table S6). The calculation predicts 18 weak transitions ($f < 0.02$) below 3.75 eV , which may explain the emergence of the tailing band above 450 nm in the experimental spectrum. These transitions consist predominantly of excitations from host occupied levels to guest virtual levels, confirming the charge-transfer character of this band. A

more intense transition at 3.76 eV ($f = 0.29$), which corresponds to the experimental maximum at ca. 480 nm, is dominated by the HOMO to L+3 excitation, which is accompanied by smaller CT contributions. This transition is red-shifted relative to its counterpart in the calculated spectrum of free **1** (3.88 eV), as indeed observed in the experiment. For [1 Δ MA⁺], the majority of frontier KS orbitals were also found to be either pure host levels (HOMO through H-6, and L+1) or pure guest levels (LUMO and L+2). The TD calculation again predicted a range of weak CT transitions (below 3.70 eV), and an intense transition of the host at 3.71 eV ($f = 0.38$), which is again red-shifted in comparison with the guest-free **1** (Figure S33, Table S5).

CONCLUSIONS

The design of the molecular squid described in this work capitalizes on structural and electronic characteristics of calixarenes, linear oligophenyls, and cycloparaphenylenes, to yield an electron-rich aromatic system that is simultaneously strained and flexible. The conformational bistability of **1**, predicted in the gas phase, leads to two types of energetically accessible geometries of the octiphenyl substructure. The possibility of switching between two curvature distributions is of general interest as a means of controlling supramolecular and optical properties of such “spring-loaded” molecular hybrids. The molecular squid shows promise both as a versatile supramolecular receptor, capable of providing an optical response upon binding of electron-deficient guests, and as a structurally nontrivial molecular porous material. By refining the present structural design, we are now trying to develop receptors in which the conformation and electronic structure of the curved π system of the host will be even more strongly affected by guest binding, to produce a functionally useful output.

ASSOCIATED CONTENT

Supporting Information

The Supporting Information is available free of charge at <https://pubs.acs.org/doi/10.1021/jacs.0c07956>.

Synthetic and spectroscopic data; additional schemes, figures, and tables; computational data; and additional references (PDF)

Crystallographic data for 5·C₆H₁₄·H₂O (CIF)

Crystallographic data for 1·3C₆H₆ (CIF)

Crystallographic data for 1·3.2CH₂Cl₂ (CIF)

Crystallographic data for [1 Δ PQ²⁺][PF₆⁻]₂·C₃H₆O (CIF)

Crystallographic data for [1 Δ DQ²⁺][PF₆⁻]₂·C₃H₆O (CIF)

Crystallographic data for [1 Δ AQ]·2.5CH₄O (CIF)

Cartesian coordinates (ZIP)

AUTHOR INFORMATION

Corresponding Author

Marcin Stępień – Wydział Chemii, Uniwersytet Wrocławski, 50-383 Wrocław, Poland; orcid.org/0000-0002-4670-8093; Email: marcin.stepien@chem.uni.wroc.pl

Authors

Rafał Frydrych – Wydział Chemii, Uniwersytet Wrocławski, 50-383 Wrocław, Poland

Tadeusz Lis – Wydział Chemii, Uniwersytet Wrocławski, 50-383 Wrocław, Poland

Wojciech Bury – Wydział Chemii, Uniwersytet Wrocławski, 50-383 Wrocław, Poland; orcid.org/0000-0002-8207-1384

Joanna Cybińska – Wydział Chemii, Uniwersytet Wrocławski, 50-383 Wrocław, Poland; PORT—Polski Ośrodek Rozwoju Technologii, 54-066 Wrocław, Poland

Complete contact information is available at: <https://pubs.acs.org/10.1021/jacs.0c07956>

Notes

The authors declare no competing financial interest.

ACKNOWLEDGMENTS

Financial support from the National Science Center of Poland (UMO-2015/19/B/ST5/00612 and UMO-2018/29/B/ST5/01842) is gratefully acknowledged. Quantum-chemical calculations were performed in the Wrocław Center for Networking and Supercomputing.

REFERENCES

- (1) Lu, D.; Huang, Q.; Wang, S.; Wang, J.; Huang, P.; Du, P. The Supramolecular Chemistry of Cycloparaphenylenes and Their Analogs. *Front. Chem.* **2019**, *7*, 668.
- (2) Leonhardt, E. J.; Jasti, R. Emerging Applications of Carbon Nanohoops. *Nat. Rev. Chem.* **2019**, *3* (12), 672–686.
- (3) Xu, Y.; Delius, M. The Supramolecular Chemistry of Strained Carbon Nanohoops. *Angew. Chem., Int. Ed.* **2020**, *59* (2), 559–573.
- (4) Kawase, T.; Tanaka, K.; Seirai, Y.; Shiono, N.; Oda, M. Complexation of Carbon Nanorings with Fullerenes: Supramolecular Dynamics and Structural Tuning for a Fullerene Sensor. *Angew. Chem., Int. Ed.* **2003**, *42* (45), 5597–5600.
- (5) Iwamoto, T.; Watanabe, Y.; Sadahiro, T.; Haino, T.; Yamago, S. Size-Selective Encapsulation of C₆₀ by [10]Cycloparaphenylene: Formation of the Shortest Fullerene-Peapod. *Angew. Chem., Int. Ed.* **2011**, *50* (36), 8342–8344.
- (6) Xia, J.; Bacon, J. W.; Jasti, R. Gram-Scale Synthesis and Crystal Structures of [8]- and [10]CPP, and the Solid-State Structure of C₆₀@[10]CPP. *Chem. Sci.* **2012**, *3* (10), 3018–3021.
- (7) Isobe, H.; Hitosugi, S.; Yamasaki, T.; Iizuka, R. Molecular Bearings of Finite Carbon Nanotubes and Fullerenes in Ensemble Rolling Motion. *Chem. Sci.* **2013**, *4* (3), 1293–1297.
- (8) Rio, J.; Beeck, S.; Rotas, G.; Ahles, S.; Jacquemin, D.; Tagmatarchis, N.; Ewels, C.; Wegner, H. A. Electronic Communication between Two [10]Cycloparaphenylenes and Bis(Azafullerene) (C₅₉N)₂ Induced by Cooperative Complexation. *Angew. Chem., Int. Ed.* **2018**, *57* (23), 6930–6934.
- (9) Sun, Z.; Ikemoto, K.; Fukunaga, T. M.; Koretsune, T.; Arita, R.; Sato, S.; Isobe, H. Finite Phenine Nanotubes with Periodic Vacancy Defects. *Science* **2019**, *363* (6423), 151–155.
- (10) Xu, Y.; Gsänger, S.; Minameyer, M. B.; Imaz, I.; Maspoch, D.; Shyshov, O.; Schwer, F.; Ribas, X.; Drewello, T.; Meyer, B.; von Delius, M. Highly Strained, Radially π -Conjugated Porphyrinylene Nanohoops. *J. Am. Chem. Soc.* **2019**, *141* (46), 18500–18507.
- (11) Huang, Q.; Zhuang, G.; Jia, H.; Qian, M.; Cui, S.; Yang, S.; Du, P. Photoconductive Curved-Nanographene/Fullerene Supramolecular Heterojunctions. *Angew. Chem., Int. Ed.* **2019**, *58* (19), 6244–6249.
- (12) Lampart, S.; Roch, L. M.; Dutta, A. K.; Wang, Y.; Warshamane, R.; Finke, A. D.; Linden, A.; Baldrige, K. K.; Siegel, J. S. Pentaindenocorannulene: Properties, Assemblies, and C₆₀ Complex. *Angew. Chem., Int. Ed.* **2016**, *55* (47), 14648–14652.
- (13) Ikemoto, K.; Kobayashi, R.; Sato, S.; Isobe, H. Entropy-Driven Ball-in-Bowl Assembly of Fullerene and Geodesic Phenylene Bowl. *Org. Lett.* **2017**, *19* (9), 2362–2365.
- (14) Majewski, M. A.; Hong, Y.; Lis, T.; Gregoliński, J.; Chmielewski, P. J.; Cybińska, J.; Kim, D.; Stępień, M. Octulene: A

Hyperbolic Molecular Belt That Binds Chloride Anions. *Angew. Chem., Int. Ed.* **2016**, *55* (45), 14072–14076.

(15) He, L.; Ng, C.-F.; Li, Y.; Liu, Z.; Kuck, D.; Chow, H.-F. Trefoil-Shaped Porous Nanographenes Bearing a Tribenzotriquinacene Core by Three-Fold Scholl Macrocyclization. *Angew. Chem., Int. Ed.* **2018**, *57* (41), 13635–13639.

(16) Miyajima, D.; Tashiro, K.; Araoka, F.; Takezoe, H.; Kim, J.; Kato, K.; Takata, M.; Aida, T. Liquid Crystalline Corannulene Responsive to Electric Field. *J. Am. Chem. Soc.* **2009**, *131* (1), 44–45.

(17) Ikemoto, K.; Kobayashi, R.; Sato, S.; Isobe, H. Synthesis and Bowl-in-Bowl Assembly of a Geodesic Phenylene Bowl. *Angew. Chem., Int. Ed.* **2017**, *56* (23), 6511–6514.

(18) Sakamoto, H.; Fujimori, T.; Li, X.; Kaneko, K.; Kan, K.; Ozaki, N.; Hijikata, Y.; Irle, S.; Itami, K. Cycloparaphenylene as a Molecular Porous Carbon Solid with Uniform Pores Exhibiting Adsorption-Induced Softness. *Chem. Sci.* **2016**, *7* (7), 4204–4210.

(19) Schaub, T. A.; Prantl, E. A.; Kohn, J.; Bursch, M.; Marshall, C. R.; Leonhardt, E. J.; Lovell, T. C.; Zakharov, L. N.; Brozek, C. K.; Waldvogel, S. R.; Grimme, S.; Jasti, R. Exploration of the Solid-State Sorption Properties of Shape-Persistent Macrocyclic Nanocarbons as Bulk Materials and Small Aggregates. *J. Am. Chem. Soc.* **2020**, *142* (19), 8763–8775.

(20) Xu, Y.; Kaur, R.; Wang, B.; Minameyer, M. B.; Gsänger, S.; Meyer, B.; Drewello, T.; Guldi, D. M.; von Delius, M. Concave-Convex π - π Template Approach Enables the Synthesis of [10]-Cycloparaphenylene-Fullerene [2]Rotaxanes. *J. Am. Chem. Soc.* **2018**, *140* (41), 13413–13420.

(21) Van Raden, J. M.; White, B. M.; Zakharov, L. N.; Jasti, R. Nanohoop Rotaxanes from Active Metal Template Syntheses and Their Potential in Sensing Applications. *Angew. Chem., Int. Ed.* **2019**, *58* (22), 7341–7345.

(22) Zhang, W.; Abdulkarim, A.; Golling, F. E.; Räder, H. J.; Müllen, K. Cycloparaphenylenes and Their Catenanes: Complex Macrocycles Unveiled by Ion Mobility Mass Spectrometry. *Angew. Chem., Int. Ed.* **2017**, *56* (10), 2645–2648.

(23) Fan, Y.-Y.; Chen, D.; Huang, Z.-A.; Zhu, J.; Tung, C.-H.; Wu, L.-Z.; Cong, H. An Isolable Catenane Consisting of Two Möbius Conjugated Nanohoops. *Nat. Commun.* **2018**, *9* (1), 3037.

(24) Segawa, Y.; Kuwayama, M.; Hijikata, Y.; Fushimi, M.; Nishihara, T.; Pirillo, J.; Shirasaki, J.; Kubota, N.; Itami, K. Topological Molecular Nanocarbons: All-Benzene Catenane and Trefoil Knot. *Science* **2019**, *365* (6450), 272–276.

(25) Segawa, Y.; Kuwayama, M.; Itami, K. Synthesis and Structure of [9]Cycloparaphenylene Catenane: An All-Benzene Catenane Consisting of Small Rings. *Org. Lett.* **2020**, *22* (3), 1067–1070.

(26) Majewski, M. A.; Stępień, M. Bowls, Hoops, and Saddles: Synthetic Approaches to Curved Aromatic Molecules. *Angew. Chem., Int. Ed.* **2019**, *58* (1), 86–116.

(27) Segawa, Y.; Yagi, A.; Matsui, K.; Itami, K. Design and Synthesis of Carbon Nanotube Segments. *Angew. Chem., Int. Ed.* **2016**, *55* (17), 5136–5158.

(28) Wu, Y.-T.; Siegel, J. S. Aromatic Molecular-Bowl Hydrocarbons: Synthetic Derivatives, Their Structures, and Physical Properties. *Chem. Rev.* **2006**, *106* (12), 4843–4867.

(29) Pun, S. H.; Miao, Q. Toward Negatively Curved Carbons. *Acc. Chem. Res.* **2018**, *51* (7), 1630–1642.

(30) Senthilkumar, K.; Kondratowicz, M.; Lis, T.; Chmielewski, P. J.; Cybińska, J.; Zafra, J. L.; Casado, J.; Vives, T.; Crassous, J.; Favereau, L.; Stępień, M. Lemniscular [16]Cycloparaphenylene: A Radially Conjugated Figure-Eight Aromatic Molecule. *J. Am. Chem. Soc.* **2019**, *141* (18), 7421–7427.

(31) Nishigaki, S.; Shibata, Y.; Nakajima, A.; Okajima, H.; Masumoto, Y.; Osawa, T.; Muranaka, A.; Sugiyama, H.; Horikawa, A.; Uekusa, H.; Koshino, H.; Uchiyama, M.; Sakamoto, A.; Tanaka, K. Synthesis of Belt- and Möbius-Shaped Cycloparaphenylenes by Rhodium-Catalyzed Alkyne Cyclotrimerization. *J. Am. Chem. Soc.* **2019**, *141* (38), 14955–14960.

(32) Rickhaus, M.; Jirasek, M.; Tejerina, L.; Gottfredsen, H.; Peeks, M. D.; Haver, R.; Jiang, H.-W.; Claridge, T. D. W.; Anderson, H. L. Global Aromaticity at the Nanoscale. *Nat. Chem.* **2020**, *12*, 236.

(33) Fernández-García, J. M.; Evans, P. J.; Filippone, S.; Herranz, M. Á.; Martín, N. Chiral Molecular Carbon Nanostructures. *Acc. Chem. Res.* **2019**, *52* (6), 1565–1574.

(34) Golder, M. R.; Jasti, R. Syntheses of the Smallest Carbon Nanohoops and the Emergence of Unique Physical Phenomena. *Acc. Chem. Res.* **2015**, *48* (3), 557–566.

(35) Lovell, T. C.; Colwell, C. E.; Zakharov, L. N.; Jasti, R. Symmetry Breaking and the Turn-on Fluorescence of Small, Highly Strained Carbon Nanohoops. *Chem. Sci.* **2019**, *10* (13), 3786–3790.

(36) Lovell, T. C.; Garrison, Z. R.; Jasti, R. Synthesis, Characterization, and Computational Investigation of Bright Orange-Emitting Benzo[1,2-c:4,5-c']diazole [10]Cycloparaphenylene. *Angew. Chem., Int. Ed.* **2020**, *59* (34), 14363–14367.

(37) Xu, Y.; Wang, B.; Kaur, R.; Minameyer, M. B.; Bothe, M.; Drewello, T.; Guldi, D. M.; von Delius, M. A Supramolecular [10]CPP Junction Enables Efficient Electron Transfer in Modular Porphyrin-[10]CPP- C_{60} Fullerene Complexes. *Angew. Chem., Int. Ed.* **2018**, *57* (36), 11549–11553.

(38) Jasti, R.; Bhattacharjee, J.; Neaton, J. B.; Bertozzi, C. R. Synthesis, Characterization, and Theory of [9]-, [12]-, and [18]-Cycloparaphenylene: Carbon Nanohoop Structures. *J. Am. Chem. Soc.* **2008**, *130* (52), 17646–17647.

(39) Takaba, H.; Omachi, H.; Yamamoto, Y.; Bouffard, J.; Itami, K. Selective Synthesis of [12]Cycloparaphenylene. *Angew. Chem., Int. Ed.* **2009**, *48* (33), 6112–6116.

(40) Yamago, S.; Watanabe, Y.; Iwamoto, T. Synthesis of [8]Cycloparaphenylene from a Square-Shaped Tetranuclear Platinum Complex. *Angew. Chem., Int. Ed.* **2010**, *49* (4), 757–759.

(41) Ball, M.; Fowler, B.; Li, P.; Joyce, L. A.; Li, F.; Liu, T.; Paley, D.; Zhong, Y.; Li, H.; Xiao, S.; Ng, F.; Steigerwald, M. L.; Nuckolls, C. Chiral Conjugated Corrals. *J. Am. Chem. Soc.* **2015**, *137* (31), 9982–9987.

(42) Ball, M.; Zhong, Y.; Fowler, B.; Zhang, B.; Li, P.; Etkin, G.; Paley, D. W.; Decatur, J.; Dalsania, A. K.; Li, H.; Xiao, S.; Ng, F.; Steigerwald, M. L.; Nuckolls, C. Macrocyclization in the Design of Organic N-Type Electronic Materials. *J. Am. Chem. Soc.* **2016**, *138* (39), 12861–12867.

(43) Della Sala, P.; Talotta, C.; Capobianco, A.; Soriente, A.; De Rosa, M.; Neri, P.; Gaeta, C. Synthesis, Optoelectronic, and Supramolecular Properties of a Calix[4]Arene-Cycloparaphenylene Hybrid Host. *Org. Lett.* **2018**, *20* (23), 7415–7418.

(44) Della Sala, P.; Talotta, C.; Caruso, T.; De Rosa, M.; Soriente, A.; Neri, P.; Gaeta, C. Tuning Cycloparaphenylene Host Properties by Chemical Modification. *J. Org. Chem.* **2017**, *82* (18), 9885–9889.

(45) Lu, D.; Zhuang, G.; Jia, H.; Wang, J.; Huang, Q.; Cui, S.; Du, P. A Novel Symmetrically Multifunctionalized Dodecamethoxy-Cycloparaphenylene: Synthesis, Photophysical, and Supramolecular Properties. *Org. Chem. Front.* **2018**, *5* (9), 1446–1451.

(46) Leonhardt, E. J.; Van Raden, J. M.; Miller, D.; Zakharov, L. N.; Alemán, B.; Jasti, R. A Bottom-Up Approach to Solution-Processed, Atomically Precise Graphitic Cylinders on Graphite. *Nano Lett.* **2018**, *18* (12), 7991–7997.

(47) Hashimoto, S.; Kayahara, E.; Mizuhata, Y.; Tokitoh, N.; Takeuchi, K.; Ozawa, F.; Yamago, S. Synthesis and Physical Properties of Polyfluorinated Cycloparaphenylenes. *Org. Lett.* **2018**, *20* (18), 5973–5976.

(48) Linnane, P.; James, T. D.; Shinkai, S. The Synthesis and Properties of a Calixarene-Based ‘Sugar Bowl’. *J. Chem. Soc., Chem. Commun.* **1995**, No. 19, 1997–1998.

(49) Evans, D. R.; Huang, M.; Fettinger, J. C.; Williams, T. L. Synthesis and Characterization of Diametrically Substituted Tetra-*O*-*n*-Butylcalix[4]Arene Ligands and Their Chelated Complexes of Titanium, Molybdenum, and Palladium. *Inorg. Chem.* **2002**, *41* (23), 5986–6000.

(50) Patel, V. K.; Kayahara, E.; Yamago, S. Practical Synthesis of [*n*]Cycloparaphenylenes (*n* = 5, 7–12) by H_2SnCl_4 -Mediated

Aromatization of 1,4-Dihydroxycyclo-2,5-Diene Precursors. *Chem. - Eur. J.* **2015**, *21*, 5742–5749.

(51) Pracht, P.; Bohle, F.; Grimme, S. Automated Exploration of the Low-Energy Chemical Space with Fast Quantum Chemical Methods. *Phys. Chem. Chem. Phys.* **2020**, *22* (14), 7169–7192.

(52) Grimme, S.; Bannwarth, C.; Shushkov, P. A Robust and Accurate Tight-Binding Quantum Chemical Method for Structures, Vibrational Frequencies, and Noncovalent Interactions of Large Molecular Systems Parametrized for All Spd-Block Elements ($Z = 1-86$). *J. Chem. Theory Comput.* **2017**, *13* (5), 1989–2009.

(53) Bannwarth, C.; Ehlert, S.; Grimme, S. GFN2-XTB—An Accurate and Broadly Parametrized Self-Consistent Tight-Binding Quantum Chemical Method with Multipole Electrostatics and Density-Dependent Dispersion Contributions. *J. Chem. Theory Comput.* **2019**, *15* (3), 1652–1671.

(54) Haddon, R. C.; Scott, L. T. π -Orbital Conjugation and Rehybridization in Bridged Annulenes and Deformed Molecules in General: π -Orbital Axis Vector Analysis. *Pure Appl. Chem.* **1986**, *58* (1), 137–142.

(55) Scott, L. T.; Jackson, E. A.; Zhang, Q.; Steinberg, B. D.; Bancu, M.; Li, B. A Short, Rigid, Structurally Pure Carbon Nanotube by Stepwise Chemical Synthesis. *J. Am. Chem. Soc.* **2012**, *134* (1), 107–110.

(56) Myśliwiec, D.; Kondratowicz, M.; Lis, T.; Chmielewski, P. J.; Stępień, M. Highly Strained Nonclassical Nanotube End-Caps. A Single-Step Solution Synthesis from Strain-Free, Non-Macrocyclic Precursors. *J. Am. Chem. Soc.* **2015**, *137* (4), 1643–1649.

(57) Quan, M. L. C.; Cram, D. J. Constrictive Binding of Large Guests by a Hemarcerand Containing Four Portals. *J. Am. Chem. Soc.* **1991**, *113* (7), 2754–2755.

(58) Juríček, M.; Barnes, J. C.; Dale, E. J.; Liu, W.-G.; Strutt, N. L.; Bruns, C. J.; Vermeulen, N. A.; Ghooray, K. C.; Sarjeant, A. A.; Stern, C. L.; Botros, Y. Y.; Goddard, W. A.; Stoddart, J. F. Ex2Box: Interdependent Modes of Binding in a Two-Nanometer-Long Synthetic Receptor. *J. Am. Chem. Soc.* **2013**, *135* (34), 12736–12746.

(59) Wu, H.; Chen, Y.; Zhang, L.; Anamimoghadam, O.; Shen, D.; Liu, Z.; Cai, K.; Pezzato, C.; Stern, C. L.; Liu, Y.; Stoddart, J. F. A Dynamic Tetracationic Macrocyclic Exhibiting Photoswitchable Molecular Encapsulation. *J. Am. Chem. Soc.* **2019**, *141* (3), 1280–1289.

(60) Inokuchi, F.; Araki, K.; Shinkai, S. Facile Detection of Cation- π Interactions in Calix[n]Arenes by Mass Spectrometry. *Chem. Lett.* **1994**, *23* (8), 1383–1386.

(61) Ranganathan, D.; Thomas, A.; Haridas, V.; Kurur, S.; Madhusudan, K. P.; Roy, R.; Kunwar, A. C.; Sarma, A. V. S.; Vairamani, M.; Sarma, K. D. Design, Synthesis, and Characterization of Tyrosinophanes, a Novel Family of Aromatic-Bridged Tyrosine-Based Cyclodepsipeptides. *J. Org. Chem.* **1999**, *64* (10), 3620–3629.

(62) Jagadesan, P.; Mondal, B.; Parthasarathy, A.; Rao, V. J.; Ramamurthy, V. Photochemical Reaction Containers as Energy and Electron-Transfer Agents. *Org. Lett.* **2013**, *15* (6), 1326–1329.

(63) Wang, P.; Yao, Y.; Xue, M. A Novel Fluorescent Probe for Detecting Paraquat and Cyanide in Water Based on Pillar[5]Arene/10-Methylacridinium Iodide Molecular Recognition. *Chem. Commun.* **2014**, *50* (39), 5064–5067.

(64) Wang, Q.; Xia, B.; Xu, J.; Tian, L.; Cheng, M.; Jiang, J. Reversible Switching of a Fluorescent Host-Guest System: Cryptand Interchange between Two Different Recognition Sites by Regulating on Guest Molecule. *Dyes Pigm.* **2018**, *159*, 513–516.

(65) Hu, G.; Yang, C.; Liu, H.; Shen, J. Pillar[5]Arene-Functionalized Paper as a Fluorescent Sensor for Cyanide Ions in Water. *New J. Chem.* **2019**, *43* (29), 11473–11476.

(66) Allwood, B. L.; Kohnke, F. H.; Stoddart, J. F.; Williams, D. J. A Macrobicyclic Receptor Molecule for the Diquat Dication. *Angew. Chem., Int. Ed. Engl.* **1985**, *24* (7), 581–584.

(67) Allwood, B. L.; Colquhoun, H. M.; Doughty, S. M.; Kohnke, F. H.; Slawin, A. M. Z.; Stoddart, J. F.; Williams, D. J.; Zarzycki, R. A. Comparison of the Receptor Stereochemistry in $[\text{Pt}(\text{Bipy})(\text{NH}_3)_2 \cdot \text{dinaphtho-30-Crown-10}][\text{PF}_6]_2$ and $[\text{Diquat-dinaphtho-30-Crown-10}][\text{PF}_6]_2$ (Bipy = 2,2'-Bipyridine). *J. Chem. Soc., Chem. Commun.* **1987**, 1054–1058.

(68) Allwood, B. L.; Spencer, N.; Shahriari-Zavareh, H.; Stoddart, J. F.; Williams, D. J. Complexation of Diquat by a Bisparaphenylene-34-Crown-10 Derivative. *J. Chem. Soc., Chem. Commun.* **1987**, No. 14, 1061.

(69) Ashton, P. R.; Slawin, A. M. Z.; Spencer, N.; Stoddart, J. F.; Williams, D. J. Complex Formation between Bisparaphenylene-(3n+4)-Crown-n Ethers and the Paraquat and Diquat Dications. *J. Chem. Soc., Chem. Commun.* **1987**, No. 14, 1066.

(70) Beer, P. D.; Tite, E. L.; Ibbotson, A. Novel Benzo Crown Ether Cavitand and Benzo Crown Ether-Ferrocenyl Host Molecules That Bind Bipyridinium and Sodium Guest Cations. *J. Chem. Soc., Chem. Commun.* **1989**, No. 24, 1874–1876.

(71) Han, T.; Chen, C.-F. Formation of Ternary Complexes between a Macrotricyclic Host and Hetero-Guest Pairs: An Acid-Base Controlled Selective Complexation Process. *Org. Lett.* **2007**, *9* (21), 4207–4210.

(72) Han, T.; Zong, Q.-S.; Chen, C.-F. Complexation of Triptycene-Based Cylindrical Macrotricyclic Polyether toward Diquaternary Salts: Ion-Controlled Binding and Release of the Guests. *J. Org. Chem.* **2007**, *72* (8), 3108–3111.

(73) Huang, F.; Slebodnick, C.; Switek, K. A.; Gibson, H. W. Inclusion [2]Complexes Based on the Cryptand/Diquat Recognition Motif. *Tetrahedron* **2007**, *63* (13), 2829–2839.

(74) He, C.; Shi, Z.; Zhou, Q.; Li, S.; Li, N.; Huang, F. Syntheses of Cis- and Trans-Dibenzo-30-Crown-10 Derivatives via Regioselective Routes and Their Complexations with Paraquat and Diquat. *J. Org. Chem.* **2008**, *73* (15), 5872–5880.

(75) Zhang, J.; Zhai, C.; Wang, F.; Zhang, C.; Li, S.; Zhang, M.; Li, N.; Huang, F. A Bis(m-Phenylene)-32-Crown-10-Based Fluorescence Chemosensor for Paraquat and Diquat. *Tetrahedron Lett.* **2008**, *49* (34), 5009–5012.

(76) Li, S.; Huang, F.; Slebodnick, C.; Ashraf-Khorassani, M.; Gibson, H. W. Complexes of Diquat with Dibenzo-24-Crown-8. *Chin. J. Chem.* **2009**, *27* (9), 1777–1781.

(77) Yan, X.; Zhang, M.; Wei, P.; Zheng, B.; Chi, X.; Ji, X.; Huang, F. PH-Responsive Assembly and Disassembly of a Supramolecular Cryptand-Based Pseudorotaxane Driven by π - π Stacking Interaction. *Chem. Commun.* **2011**, *47* (35), 9840.

(78) Chi, X.; Xue, M.; Ma, Y.; Yan, X.; Huang, F. A Pillar[6]Arene with Mono(Ethylene Oxide) Substituents: Synthesis and Complexation with Diquat. *Chem. Commun.* **2013**, *49* (74), 8175.

(79) Han, Y.; Cao, J.; Li, P.-F.; Zong, Q.-S.; Zhao, J.-M.; Guo, J.-B.; Xiang, J.-F.; Chen, C.-F. Complexation of Triptycene-Derived Macrotricyclic Polyether with Paraquat Derivatives, Diquat, and a 2,7-Diazapyrenium Salt: Guest-Induced Conformational Changes of the Host. *J. Org. Chem.* **2013**, *78* (7), 3235–3242.

(80) Guo, Q.-H.; Zhao, L.; Wang, M.-X. Synthesis and Molecular Recognition of Water-Soluble S6-Corona[3]Arene[3]Pyridazines. *Angew. Chem., Int. Ed.* **2015**, *54* (29), 8386–8389.

(81) Xu, M.; Chen, L.; Jia, Y.; Mao, L.; Feng, W.; Ren, Y.; Yuan, L. A Rare Case for Binding a Diquat Salt by Two Cyclo[6]Aramides. *Supramol. Chem.* **2015**, *27* (5–6), 436–443.

(82) Guo, Q.-H.; Zhao, L.; Wang, M.-X. Synthesis, Structure, and Molecular Recognition of S6- and (SO₂)6-Corona[6](Het)Arenes: Control of Macrocyclic Conformation and Properties by the Oxidation State of the Bridging Heteroatoms. *Chem. - Eur. J.* **2016**, *22* (20), 6947–6955.

(83) Niu, Z.; Price, T. L.; Slebodnick, C.; Gibson, H. W. Pseudocryptand-Type Complexes of Heterocyclic Derivatives of Bis(Meta-Phenylene)-32-Crown-10 with Diquat. *Tetrahedron Lett.* **2016**, *57* (1), 60–63.

(84) Xu, Z.; Chen, M.; Liang, J.; Zhang, S.; Guo, M.; Li, Y.; Jiang, L. High-Yield Preparation of New Crown Ether-Based Cryptands and Improving Complexation with Paraquat, Paraquat Derivatives and Diquat. *Tetrahedron* **2016**, *72* (49), 8009–8014.

(85) Pederson, A. M.-P.; Price, T. L.; Slebodnick, C.; Schoonover, D. V.; Gibson, H. W. The Long and the Short of It: Regiospecific

Syntheses of Isomers of Dicarbomethoxydibenzo-27-Crown-9 and Binding Abilities of Their Pyridyl Cryptands. *J. Org. Chem.* **2017**, *82* (16), 8489–8496.

(86) Jones, J. W.; Price, T. L.; Huang, F.; Zakharov, L.; Rheingold, A. L.; Slebodnick, C.; Gibson, H. W. Pseudocryptand Hosts for Paraquats and Diquats. *J. Org. Chem.* **2018**, *83* (2), 823–834.

(87) Pederson, A. M.-P.; Price, T. L.; Schoonover, D. V.; Slebodnick, C.; Gibson, H. W. Reverse^π Pyridyl Cryptands as Hosts for Viologens. *Heteroat. Chem.* **2018**, *29* (3), No. e21422.

(88) Vidal-Vidal, A.; Cabaleiro-Lago, E. M.; Silva López, C.; Faza, O. N. Rational Design of Efficient Environmental Sensors: Ring-Shaped Nanostructures Can Capture Quat Herbicides. *ACS Omega* **2018**, *3* (12), 16976–16988.

(89) Zhao, M.-Y.; Guo, Q.-H.; Wang, M.-X. Understanding the Driving Force for the Molecular Recognition of S6-Corona[3]-Arene[3]Pyridazine toward Organic Ammonium Cations. *Org. Chem. Front.* **2018**, *5* (5), 760–764.

(90) Ma, Y.; Chi, X.; Yan, X.; Liu, J.; Yao, Y.; Chen, W.; Huang, F.; Hou, J.-L. Per-Hydroxylated Pillar[6]Arene: Synthesis, X-Ray Crystal Structure, and Host-Guest Complexation. *Org. Lett.* **2012**, *14* (6), 1532–1535.

(91) Li, Z.; Liu, G.; Xue, W.; Wu, D.; Yang, Y.-W.; Wu, J.; Liu, S. H.; Yoon, J.; Yin, J. Construction of Hetero[*n*]Rotaxanes by Use of Polyfunctional Rotaxane Frameworks. *J. Org. Chem.* **2013**, *78* (22), 11560–11570.

(92) Wei, P.; Wang, H.; Jie, K.; Huang, F. Taco Complex-Templated Highly Regio- and Stereo-Selective Photodimerization of a Coumarin-Containing Crown Ether. *Chem. Commun.* **2017**, *53* (10), 1688–1691.

(93) Kawano, M.; Fujita, M. Direct Observation of Crystalline-State Guest Exchange in Coordination Networks. *Coord. Chem. Rev.* **2007**, *251* (21–24), 2592–2605.

(94) Lin, J. B.; Darzi, E. R.; Jasti, R.; Yavuz, I.; Houk, K. N. Solid-State Order and Charge Mobility in [5]- to [12]Cycloparaphenylenes. *J. Am. Chem. Soc.* **2019**, *141* (2), 952–960.

(95) McMorran, D. A.; Steel, P. J. The First Coordinatively Saturated, Quadruply Stranded Helicate and Its Encapsulation of a Hexafluorophosphate Anion. *Angew. Chem., Int. Ed.* **1998**, *37* (23), 3295–3297.

(96) Siegel, J. S.; Anet, F. A. L. Dichlorofluoromethane-*d*: A Versatile Solvent for VT-NMR Experiments. *J. Org. Chem.* **1988**, *53* (11), 2629–2630.

(97) Tan, L.-L.; Li, H.; Tao, Y.; Zhang, S. X.-A.; Wang, B.; Yang, Y.-W. Pillar[5]Arene-Based Supramolecular Organic Frameworks for Highly Selective CO₂-Capture at Ambient Conditions. *Adv. Mater.* **2014**, *26* (41), 7027–7031.

(98) Sarkisov, L.; Harrison, A. Computational Structure Characterisation Tools in Application to Ordered and Disordered Porous Materials. *Mol. Simul.* **2011**, *37* (15), 1248–1257.

(99) Ongari, D.; Boyd, P. G.; Barthel, S.; Witman, M.; Haranczyk, M.; Smit, B. Accurate Characterization of the Pore Volume in Microporous Crystalline Materials. *Langmuir* **2017**, *33* (51), 14529–14538.

(100) Yanai, T.; Tew, D. P.; Handy, N. C. A New Hybrid Exchange-Correlation Functional Using the Coulomb-Attenuating Method (CAM-B3LYP). *Chem. Phys. Lett.* **2004**, *393* (1–3), 51–57.

(101) Dreuw, A.; Head-Gordon, M. Single-Reference Ab Initio Methods for the Calculation of Excited States of Large Molecules. *Chem. Rev.* **2005**, *105* (11), 4009–4037.